

Data-centric Prediction Explanation via Kernelized Stein Discrepancy

Mahtab Sarvmaili¹ Hassan Sajjad¹ Ga Wu¹

Abstract

Existing example-based prediction explanation methods often bridge test and training data points through the model’s parameters or latent representations. While these methods offer clues to the causes of model predictions, they often exhibit innate shortcomings, such as incurring significant computational overhead or producing coarse-grained explanations. This paper presents a Highly-precise and Data-centric Explanation (HD-Explain), a straightforward prediction explanation method exploiting properties of Kernelized Stein Discrepancy (KSD). Specifically, the KSD uniquely defines a parameterized kernel function for a trained model that encodes model-dependent data correlation. By leveraging the kernel function, one can identify training samples that provide the best predictive support to a test point efficiently. We conducted thorough analyses and experiments across multiple classification domains, where we show that HD-Explain outperforms existing methods from various aspects, including 1) preciseness (fine-grained explanation), 2) consistency, and 3) computation efficiency, leading to a surprisingly simple, effective, and robust prediction explanation solution.

1. Introduction

As one of the decisive factors affecting the performance of a Machine Learning (ML) model, training data points are of great value in promoting the model’s transparency and trustworthiness, including explaining prediction results, tracing sources of errors, or summarizing the characteristics of the model (Cai et al., 2019; Anik & Bunt, 2021; Nam et al., 2022). The challenges of example-based prediction explanation mainly come from retrieving relevant data points from a vast pool of training samples or justifying the rationale of such explanations (Lim et al., 2019; Zhou et al., 2021).

Modern example-based prediction explanation methods

commonly approach the above challenges by constructing an influence chain between training and test data points (Li et al., 2020; Nam et al., 2022; Tsai et al., 2023). The influence chain could be either data points’ co-influence on model parameters or their similarity in terms of latent representations. In particular, Influence Function (Koh & Liang, 2017), one of the representative, model-aware explanation methods, looks for the shift of the model parameters (due to up-weighting each training sample) as the sample’s influence score. Since computing the inverse Hessian matrix is challenging, the approach adapts Conjugate Gradients Stochastic Estimation and the Perlmutter trick to reduce its computation cost. Representer Point Selection (RPS) (Yeh et al., 2018), as another example, reproduces the representer theorem by refining the trained neural network model with $L2$ regularization, such that the influence score of each training sample can be represented as the gradient of the predictive layer. While computationally efficient, RPS is criticized for producing coarse-grained explanations that are more class-level rather than instance-level explanations (Sui et al., 2021) (In this paper we use the instance level explanation and example-based explanation interchangeably.). Multiple later variants (Pruthi et al., 2020; Sui et al., 2021) attempted to mitigate the drawbacks above, but their improvements were often limited by the cause of their shared theoretical scalability bounds.

This paper presents Highly-precise and Data-centric Explanation (HD-Explain), a post-hoc, model-aware, example-based explanation solution for neural classifiers. Instead of relying on data co-influence on model parameters or feature representation similarity, HD-Explain retains the influence chain between training and test data points by exploiting the underrated properties of Kernelized Stein Discrepancy (KSD) between the trained predictive model and its training dataset. Specifically, we note that the Stein operator augmented kernel uniquely defines a pairwise data correlation (in the context of a trained model) whose expectation on the training dataset results in the minimum KSD (as a discrete approximation) compared to that of the dataset sampled from different distributions. By exploiting this property, we can 1) reveal a subset of training data points that provides the best predictive support to the test point and 2) identify the potential distribution mismatch among training data points. Jointly leveraging these advantages, HD-Explain can

¹Faculty of Computer Science, Dalhousie University, Canada. Correspondence to: Mahtab Sarvmaili <mahtab.sarvmaili@dal.ca>.

Table 1: Summary of existing Post-hoc Example-based Prediction Explanation Methods that work with deep neural networks. Practicality of the whole model explanation is measured by the feasibility of explaining the prediction of ResNet-18 trained on CIFAR-10 with a single A100 GPU machine. CIFAR-10 is a small benchmark data with 50000 training samples.

Method	Explanation of	Need optimization as sub-routine	Whole model explanation		Inference computation complexity bounded by	Memory/cache (of each training sample) bounded by
			Theoretical	Practical		
Influence Function	Original Model	Yes (Iterative HVP approximation)	Yes	No	1. $H_{\theta}^{-1} \nabla_{\theta} L(\mathbf{x}_t, \theta)$ approximation 2. $\langle \nabla_{\theta} L(\mathbf{x}, \theta), H_{\theta}^{-1} \nabla_{\theta} L(\mathbf{x}_t, \theta) \rangle$	Size of model parameters
RPS	Fine-tuned Model	Yes (L2 regularized last layer retrain)	No	No	1. last layer representation \mathbf{f}_t 2. $\langle \alpha_i \mathbf{f}_i, \mathbf{f}_t \rangle$	Size of model parameters of the last layer
TracIn*	Original Model	No	Yes	No	1. $\nabla_{\theta} L(\mathbf{x}_t, \theta)$ approximation 2. $\langle \nabla_{\theta} L(\mathbf{x}, \theta), \nabla_{\theta} L(\mathbf{x}_t, \theta) \rangle$	Size of model parameters
HD-Explain	Original Model	No	Yes	Yes	1. $\nabla_{\mathbf{x}_t} f(\mathbf{x}_t, \theta)_{y_t}$ 2. Closed-form $k_{\theta}(\mathbf{x}, \mathbf{x}_t)$ defined by KSD	Size of data dimension

* TracIn typically requires to access the training process. Here, TracIn* refers to a special case that only use the last training checkpoint.

produce explanations faithful to the original trained model with a corresponding confidence level.

We conducted a wide range of qualitative and quantitative experiments and analyses to demonstrate the effectiveness and efficiency of HD-Explain. Our empirical results show that the HD-Explain offers fine-grained, instance-level explanations with remarkable computational efficiency on multiple applications, compared to well-known example-based prediction explanation solutions. Given its algorithmic simplicity and scalability, we believe HD-Explain is an excellent addition to the literature on example-based prediction explanation research.

2. Preliminary and Related Work

2.1. Post-hoc Classifier Explanation by Examples

Post-hoc Classifier Explanation by Examples (a.k.a prototypes, representers) refers to a category of classifier explanation approaches that pick a subset of training data points as prediction explanations without accessing the model training process. Its research history spans from the model-intrinsic approach to the recent impact-based approach.

Model-inherent approaches are essentially a feature of self-explanatory machine learning models such as k -nearest neighbor (Peterson, 2009) or decision tree; For a given test data point, similar data points on the raw feature space can be efficiently selected as explanations through the inherent decision making mechanism of the self-explanatory machine learning models. In fact, attracted by their inherent explanatory power, multiple well-known works attempted to compile complex black-box models into self-explanatory models for enabling prediction explanation (Frosst & Hinton, 2017), while computationally inefficient.

To unlock the general explanatory power applicable to black-box models, multiple later studies suggest to fall back to statistics-based solutions, looking for prototype samples

that could represent common data points or play critical roles in data distribution. MMD-critic (Kim et al., 2016) and Normative and Comparative explanations (Cai et al., 2019) are the well-known examples in this category. Unfortunately, those approaches often overlook the characteristics of trained models, making their prediction explanations general to the training dataset rather than a trained model instance.

Recently, influence-based methods have emerged as the prevailing technique in model explanation (Li et al., 2020; Nam et al., 2022; Bae et al., 2022; Park et al., 2023). Influence function (Koh & Liang, 2017), as one of the earliest influence-based solutions, bridges the outcome of a prediction task to training data points by, first, evaluating training data’s influence on the model parameters and, then, estimating how model parameter changes affect prediction. Similarly, Representative Point Selection (RPS) (Yeh et al., 2018) builds such an influence chain by fitting the representation theorem, where the weighted product between the representations of test and training samples comes into play. Concerning the computational overhead of previous work, the later solution TracIn (Pruthi et al., 2020) proposed a simple approximation of the influence function via a first-order Taylor expansion (essentially Neural Tangent Kernel (Jacot et al., 2018)), successfully discarding the inverse Hessian matrix from the influence chain formulation. BoostIn (Brophy et al., 2023) further extends TracIn and is dedicated to interpreting the predictions of gradient-boosted decision trees. RPS-LJE (Sui et al., 2021), on the other hand, alleviated the inconsistent explanation problem of RPS through Local Jacobian Expansion. In the latest publication (Tsai et al., 2023), all of the above methods described in this paragraph are identified as special cases of *Generalized Representers* but with different chosen kernels.

One limitation of the current influence-based methods is that they attribute the influence of each training data point to the parameters of the trained model as an essential intermediate

step. Indeed, as the nature of stochastic gradient descent (the dominating training strategy of neural networks), isolating such contribution is barely possible without 1) relying on approximations or 2) accessing the training process. Unfortunately, either solution would result in performance degradation or heavy computational overhead (Schioppa et al., 2022). Hence, this work delves into the exploration of an alternative influence connection between training and test data points without exploiting the perturbation of model parameters.

2.2. Kernelized Stein Discrepancy

The idea of Kernelized Stein Discrepancy (KSD) (Liu et al., 2016) can be traced back to a theorem called Stein Identity (Kattumannil, 2009) that states, if a smooth distribution $p(x)$ and a function $\phi(x)$ satisfy $\lim_{\|x\| \rightarrow \infty} p(x)\phi(x) = 0$,

$$\mathbb{E}_{x \sim p}[\phi(x) \nabla_x \log p(x) + \nabla_x \phi(x)] = 0, \quad \forall f.$$

The above expression could be further abstracted to use function operator \mathcal{A}_p (a.k.a Stein operator) such that

$$\mathcal{A}_p \phi(x) = \phi(x) \nabla_x \log p(x) + \nabla_x \phi(x),$$

where the operator encodes distribution $p(x)$ in the form of derivative to input (a.k.a score function).

Stein’s identity offers a mechanism to measure the gap between two distributions by assuming the variable x is sampled from a different distribution $q \neq p$ such that

$$\sqrt{\mathbb{S}(q, p)} = \max_{\phi \in \mathcal{F}} \mathbb{E}_{x \sim q}[\mathcal{A}_p \phi(x)],$$

where the expression takes the most discriminant ϕ that maximizes the violation of Stein’s identity to quantify the distribution discrepancy. This discrepancy is, accordingly, referred as Stein Discrepancy.

The challenge of computing Stein Discrepancy comes from the selection of function set \mathcal{F} , which motivates the later innovation of KSD that takes \mathcal{F} to be the unit ball of a reproducing kernel Hilbert space (RKHS). By leveraging the reproducing property of RKHS, the KSD could be eventually transformed into

$$\mathbb{S}(q, p) = \mathbb{E}_{x, x' \sim q}[\kappa_p(x, x')]$$

where $\kappa_p(x, x') = \mathcal{A}_p^x \mathcal{A}_p^{x'} k(x, x')$ that can work with arbitrary kernel function $k(x, x')$. See Appendix B for expanded derivations.

In the literature, KSD has been adopted for tackling three types of application tasks – 1) parameter inference (Barr et al., 2019), 2) Goodness-of-fit tests (Chwialkowski et al., 2016; Liu et al., 2016; Yang et al., 2018), and 3) particle filtering (sampling) (Gorham et al., 2020; Korba et al., 2021).

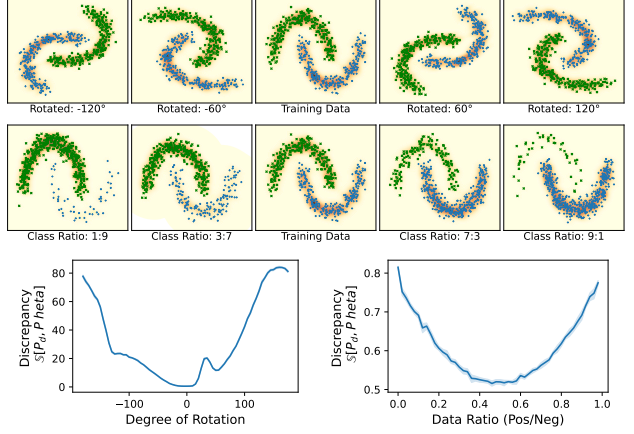


Figure 1: Varying of Kernelized Stein Discrepancy given the shift of training data distribution on Two Moon dataset.

However, to the best of our knowledge, its innate property that uniquely defines model-dependent data correlation has never been exploited, which, we note, is valuable to interpret model behaviour from various aspects, including instance-level prediction explanation and global prototypical explanations.

3. Example-based Prediction Explanation via Kernelized Stein Discrepancy (HD-Explain)

Consider a trained classifier f_θ as the outcome of a training process with Maximum Likelihood Estimation (MLE)

$$\arg\max_{\theta} \mathbb{E}_{(\mathbf{x}, y) \sim P_D} [\log P_\theta(y|\mathbf{x})].$$

Theoretically, maximizing observation likelihood is equivalent to minimizing a KL divergence between data distribution P_D and the parameterized distribution P_θ such that

$$\begin{aligned} \mathbb{D}_{\text{KL}}(P_D, P_\theta) &= \mathbb{E}_{(\mathbf{x}, y) \sim P_D} \left[\log \frac{P_D(\mathbf{x}, y)}{P_\theta(\mathbf{x}, y)} \right] \\ &= - \underbrace{\mathbb{E}_{(\mathbf{x}, y) \sim P_D} [\log P_\theta(y|\mathbf{x})]}_{\text{Likelihood}} + \underbrace{\mathbb{E}_{(\mathbf{x}, y) \sim P_D} [\log P_D(y|\mathbf{x})]}_{\text{constant}}, \end{aligned}$$

which, in turn, is proven recently to align with minimizing Stein Discrepancy in the form of gradient descent (Liu & Wang, 2016)

$$\nabla_{\theta} \mathbb{D}_{\text{KL}}(P_D, P_\theta) = -\mathbb{S}(P_D, P_\theta).$$

The chain of reasoning above shows that a well-trained classifier f_θ through gradient-descent should lead to minimum Stein Discrepancy between the training dataset distribution and the model encoded distribution $\mathbb{S}(P_D, P_\theta)$ ¹. We can

¹Since P_D is discrete distribution while P_θ is continuous, the Stein Discrepancy between the two distributions will not recap Stein Identity (= 0) with a limited number of training data points.

empirically verify the connection through simple examples as shown in Figure 1, where the changes in training data distribution would result in larger KSD compared to that of the original training data distribution. Intuitively, the connection shows that there is a tie between a model and its training data points, encoded in the form of a stein kernel function $k_\theta(\cdot, \cdot)$ defined on each pair of data points. As the kernel function is conditioned on model f_θ , we note it is an encoding of data correlation under the context of a trained model, which paves the foundation of the example-based prediction explanation as shown next.

3.1. KSD between Model and Training Data

Recall that KSD, $\mathbb{S}(P_D, P_\theta)$, defines the correlation between pairs of training samples through model θ dependent kernel function with closed-form decomposition

$$\begin{aligned} \kappa_\theta((\mathbf{x}_a, y_a), (\mathbf{x}_b, y_b)) &= \mathcal{A}_\theta^a \mathcal{A}_\theta^b k(a, b) \\ &= \nabla_a \nabla_b k(a, b) + k(a, b) \nabla_a \log P_\theta(a) \nabla_b \log P_\theta(b) \\ &\quad + \nabla_a k(a, b) \nabla_b \log P_\theta(b) + \nabla_b k(a, b) \nabla_a \log P_\theta(a), \end{aligned} \quad (1)$$

where we denote data point (\mathbf{x}_a, y_a) with a for clean notation. The only model-dependent factor in the above decomposition is a derivative $\nabla_{\mathbf{x}, y} \log P_\theta(\mathbf{x}, y)$ (for both data a or b). Hence, to utilize KSD for prediction explanation, we first need to unravel the derivative of the trained model with respect to a whole data point (including its label). Indeed, while the gradient of a classifier $\nabla_{\mathbf{x}} \log P_\theta(y|\mathbf{x})$ on its input feature \mathbf{x} is straightforward, the gradient to the entire data points is less evident due to the lack of definition of $P_\theta(\mathbf{x})$.

To obtain the joint distribution of $P_\theta(\mathbf{x}, y)$ for facilitating KSD computation, we propose to set $P_\theta(\mathbf{x}) \equiv P_D(\mathbf{x})$ as uniform distribution. Although this setting appears hasty, we note P_D represents the uniform data distribution in dataset D , which, while reflects, but is not the complex unknown distribution from which the data is sampled. In particular, for a data point (\mathbf{x}, y) in dataset D with i.i.d assumption, $P_D(\mathbf{x})$ is indeed uniformly distributed, whereas $P_D(y|\mathbf{x})$ is a delta distribution with probability 1.

With the above setting, the score function $\nabla_{\mathbf{x}, y} \log P_\theta(\mathbf{x}, y)$ in the Stein operator \mathcal{A}_θ could be derived as a concatenation of the gradient of model $f_\theta(\mathbf{x})_y$ to its input \mathbf{x} and its probabilistic prediction $f_\theta(\mathbf{x})$, since

$$\begin{aligned} \nabla_{\mathbf{x}, y} \log P_\theta(\mathbf{x}, y) &= \nabla_{\mathbf{x}, y} [\log P_\theta(y|\mathbf{x}) + \log P_d(\mathbf{x})] \\ &= \nabla_{\mathbf{x}, y} \log P_\theta(y|\mathbf{x}) + [\nabla_{\mathbf{x}} \log P_d(\mathbf{x}) || \nabla_y P_d(\mathbf{x})] \\ &= [\nabla_{\mathbf{x}} \log \mathbf{y}^\top f_\theta(\mathbf{x}) || \nabla_y \log \mathbf{y}^\top f_\theta(\mathbf{x})] + [0 || 0] \\ &= [\nabla_{\mathbf{x}} \log f_\theta(\mathbf{x})_y || f_\theta(\mathbf{x})], \end{aligned} \quad (2)$$

where $[||]$ denotes concatenation operation, and we use one-hot encoding \mathbf{y} of y to clarify the gradient computation.

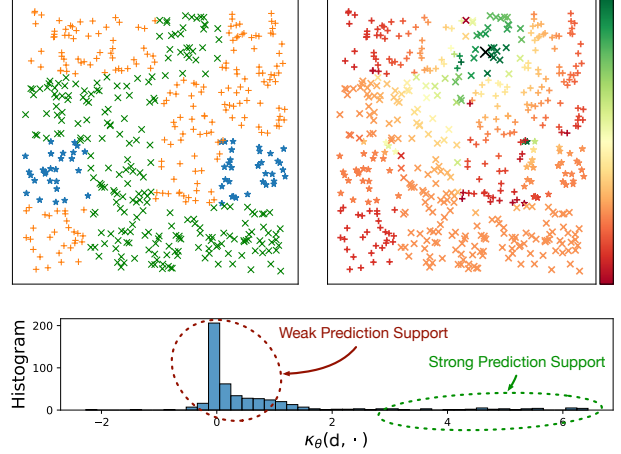


Figure 2: Demonstration of HD-Explain on 2D Rectangular synthetic dataset. Top-left shows the training dataset with three classes. Top-right shows the explanation support of training data points to a given test point (as black cross), where green shows a higher KSD kernel value. The bottom shows the distribution of KSD kernel value to the test point, where only a small number of training data points provide strong support to this prediction.

Combining Equation 1 and 2, we can estimate the correlation of any pairs of training data points conditioned on the trained machine learning model. Computationally, since a score function $\nabla_{\mathbf{x}, y} \log P_\theta(\mathbf{x}, y)$ depends on a single data point, its outputs of the training set could be pre-computed and cached for accelerate the kernel computation. In particular, the output dimension of the score function is simply $m + k$ for data with m dimensional features and k class labels. Compared to the existing solutions, whose training data cache (or influence) are bounded by the dimension of model parameters (such as Influence function, TracIn, RPS, RPS-JLE), the explanation method built on KSD would come with a significant advantage in terms of scalability. We note this statement is generally true for neural network based classifiers, whenever the size of model parameters is far larger than the data dimension.

3.2. Prediction Explanation via KSD

Now, we present how to extend the previously described kernel function to support the prediction explanation. As stated in Equation 1, computing the kernel function requires to access features and labels of a data point. While the ground-truth label information is provided in the training set, it is inaccessible during inference time given a test data point. Hence, to utilize the KSD kernel function, we place predicted class \hat{y}_t of the test point \mathbf{x}_t as a label to construct a complete data point $(\mathbf{x}_t, \hat{y}_t)$.

At this stage, searching supportive training examples for a given test point \mathbf{x}_t could be reduced to look for top-k training data points that maximize the KSD defined kernel. For top-1 explanation sample, in particular, we look for

$$\operatorname{argmax}_i \kappa_{\theta}([\mathbf{x}_t || \hat{\mathbf{y}}_t], [\mathbf{x}_i || \mathbf{y}_i]), \quad (3)$$

where, again, we use one-hot encoding for data labels.

Figure 2 demonstrates a simple example on a 2d synthetic dataset. By iterating over all training data points and evaluating $\kappa_{\theta}(\mathbf{d}, \cdot)$, we highlight that only a small number of training data points provide a strong influence on a particular prediction (see Figure 2 (bottom)).

4. Evaluations and Analysis

In this section, we conduct several qualitative and quantitative experiments to demonstrate various properties of the proposed HD-Explain solution and analyze it with existing example-based solutions to understand where and how the approach can be used in practice. Codes are available in the supplementary materials.

Datasets: We are particularly interested in classification tasks that are highly sensitive to trustworthiness and with a clear demand for prediction explanations. To this end, we designed our experiments to include multiple disease classification datasets, where diagnosis explanation is highly desired. We also introduced synthetic and benchmark classification datasets to deliver the main idea without the need for medical background knowledge. Concretely, the primary datasets used in our experiments include CIFAR-10 ($32 \times 32 \times 3$), Brain Tumor (Magnetic Resonance Imaging, $128 \times 128 \times 3$), and Ovarian Cancer (Histopathology Images, $128 \times 128 \times 3$). More details of the datasets are listed in the Appendix.

Baselines: The baseline explainers used in our experiments include Influence Function, Representer Point Selection, and TracIn. While other variants of these baseline explainers exist (Barshan et al., 2020; Sui et al., 2021; Chen et al., 2021), we note they don’t offer fundamental performance improvements over the classic ones. In addition, as Influence Function and TracIn face scalability issues, we limit the influence of parameters to the last layer of the model so that they can work with models that contain a large number of parameters. Our experiments use ResNet-18 as the backbone model architecture (with around 11 million trainable parameters) for all image datasets. Finally, we also introduce an HD-Explain variant (HD-Explain*) to match the last layer setting of other baseline models, even though HD-Explain can scale up to the whole model without computation pressure (see Appendix F for details).

Metrics: In existing example-based explanation works, the experimental results are often demonstrated qualitatively,

as visualized explanation instances, without quantitative evaluation, which, we believe, is subjective and hardly convincing. To obtain a comprehensive understanding of the effectiveness of explanation methods, we proposed several quantitative metrics in this paper.

- **Hit Rate:** Hit rate shows how likely an explanation sample hits the desired example cases. Here, the desired examples are guaranteed to be undisputed. Specifically, we modify a training data point with minor augmentations (adding noise or flipping horizontally) and use it as a test data point, such that the best explanation for the generated test data point should be the original data point in the training set.
- **Coverage:** Given n test data points, we show how many unique explanation samples an explanation method can produce when configuring to return top-k training samples. Formally,

$$\text{Coverage} = \frac{|\cup_{i=1}^n e_i|}{n \times k}$$

where e_i is the set of top-k explanations for test data point i . Larger coverage is preferred as it suggests the higher granularity (per test point) of the explanation.

- **Run Time:** Measuring the run time of explanation methods. We measure the wall clock time.

4.1. Qualitative Evaluation

Following the convention of previous contributions in the literature, we show the prediction explanation instances for all candidate approaches side by side. Figure 3 shows three test cases of the CIFAR10 classification task that cover different classification outcomes, including high-confident correct prediction, low-confident correct prediction, and low-confident incorrect prediction. For both correct prediction cases, we are confident that HD-Explain provides a better explanation than others in terms of visually matching test data points. E.g. brown frogs in Figure 3 (a) and deer on the grass in Figure 3 (b). In contrast, for the misclassified prediction case (Figure 3 (c)), we note the HD-Explain produces examples that do not even belong to the same class as the predicted one. It is a good outcome as the method is not confident in providing consistent explanations. RPS also shows such inconsistency, which aligns with its claim (Yeh et al., 2018). The other two baseline methods do not offer such properties and still produce explanations that match the predicted label well. It is hard to justify how those samples support such prediction visually (since no clear shared pattern is obvious to us). In addition, it is interesting to see that Influence Function and TracIn produce near identical explanations, reflecting their similarity in leveraging the perturbation of model parameters.

Data-centric Prediction Explanation via Kernelized Stein Discrepancy

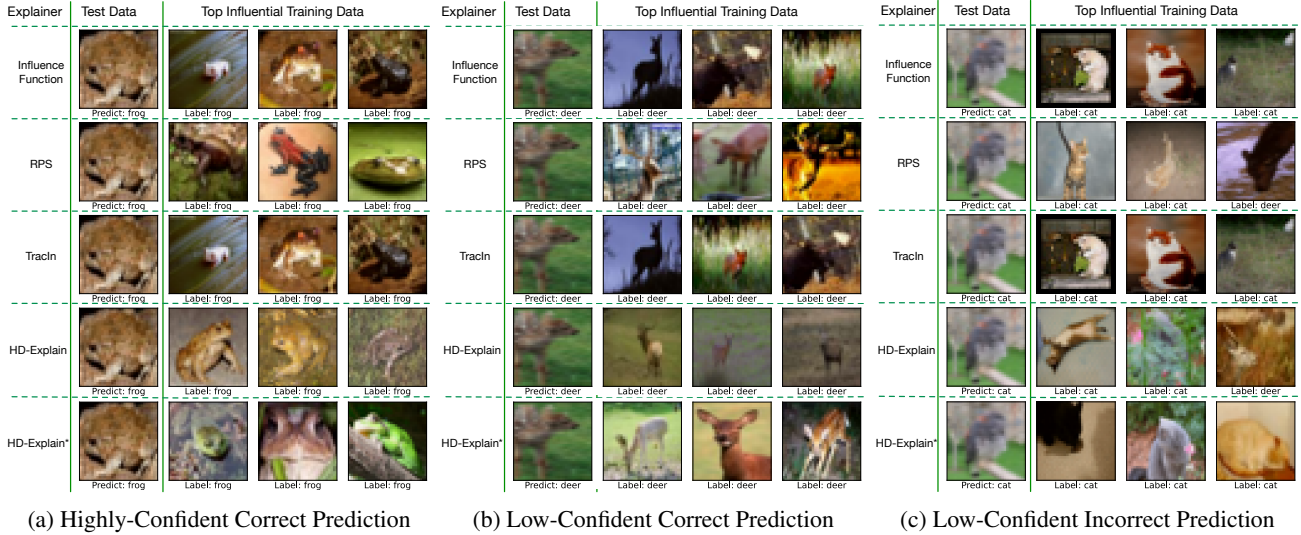


Figure 3: Qualitative explanation comparison among candidate example-based explanation methods. We show three scenarios where the target model makes 1) a highly-confident prediction that matches ground truth label, 2) a low-confident prediction that matches ground truth label, 3) low-confident prediction that does not match ground truth label (which is a bird). For each sub plot, we show top-3 influential training data points picked by the explanation methods for the test example.

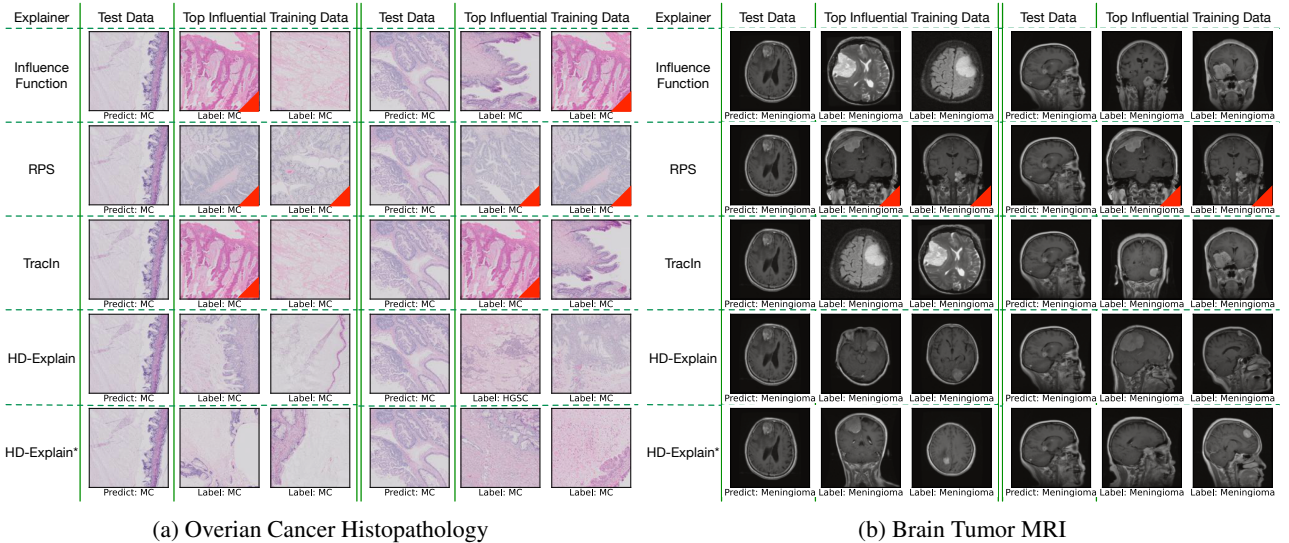


Figure 4: Qualitative explanation comparison among candidate example-based explanation methods on Overian Cancer histopathology and Brain Tumor MRI datasets. We show two test data points that are predicted to belong to the same class in each dataset. Red triangle in the top right corner of an image shows the duplicate explanations across test samples.

Figure 4 provides additional insights into Ovarian Cancer histopathology and Brain Tumor MRI datasets. HD-Explain again shows a better explanation for producing training samples that appear similar to the test samples (note, for the semantic similarity should be referred to a medical practitioner). E.g. respecting the scanning orientation of test points in MRI as shown in Figure 4 (b). We note all baseline approaches tend to produce similar explanations to test

samples belonging to the same classes. Rather than providing individual prediction explanations, those approaches act closer to per-class interpreters that look for class prototypes. To verify this observation further, we conducted a quantitative evaluation, as described in the next section.

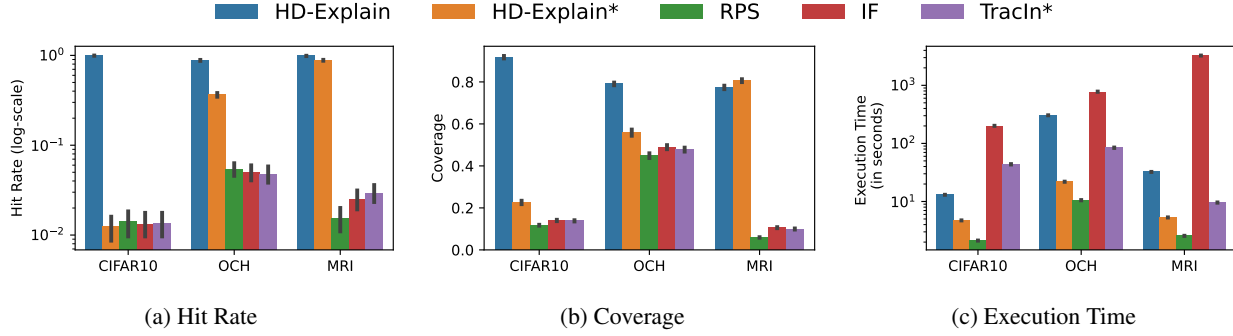


Figure 5: Quantitative explanation comparison among candidate example-based explanation methods. Data augmentation strategy used is Noise Injection. Error bar shows 95% confidence interval.

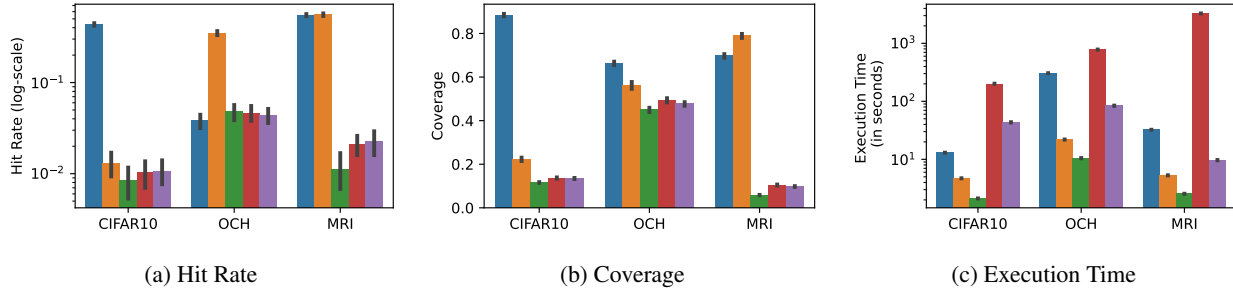


Figure 6: Quantitative explanation comparison among candidate example-based explanation methods. Data augmentation strategy used is Horizontal Flip. Error bar shows 95% confidence interval. We reuse the legend of Figure 5.

4.2. Quantitative Evaluation

Now, we aim to evaluate the performance of the candidate explanation method through quantitative analysis. As explainability is often subjective, we limit our experiments to training datasets where ground-truth explanation samples are available to obtain fair evaluation results. Specifically, given a training data sample (\mathbf{x}_i, y_i) , we generate a test point \mathbf{x}_t by adopting two image data augmentation methods:

- **Noise Injection:** $\mathbf{x}_t = \mathbf{x}_i + \epsilon$ s.t. $\epsilon \sim \mathcal{N}(0, 0.01\sigma)$, where σ is the element-wise standard deviation of features in the entire training dataset.
- **Horizontal Flip:** $\mathbf{x}_t = \text{flip}(\mathbf{x}_i)$, where we flip images horizontally that do not compromise the semantic meaning of images for the three datasets.

Since the data augmentation is guaranteed to maintain prediction consistency, the ideally best explanation for the generated test point is the original data point \mathbf{x}_i itself, considering their similarity. Hence, the quantitative evaluation could be a sample retrieval evaluation where **Hit Rate** measures the probability of successful retrieval. To provide reliable statistics, we created 30 augmented test points for each training data point ($> 10,000$ data points) in each dataset, resulting in more than 300,000 independent runs.

Figure 5(a) shows the hit rate comparison among candidate

methods on the three image classification datasets under Noise Injection data augmentation. It was surprising to observe that existing methods face significant difficulty in retrieving the idea explanatory sample ($\leq 10\%$), even with such a simple problem setup; only HD-Explain (and its variant) produces a reasonable successful rate ($> 80\%$). This observation raised our curiosity to know the underlying reason. Figure 5(b) shows the following experiments where we compute **Coverage** of unique explanations. The metric, coverage, shows the ratio of explanation samples that are unique over many test points. The purpose is to understand how likely a user may receive instance-specific explanations if they have many test points to interpret. It turns out existing solutions produce only 10% - 50% coverage – many test points receive the same set of explanations, disregarding their unique characteristic. This result reflects our previous observation in Figure 4, where we saw multiple duplicated explanations (as shown with red corner tags). In fact, the explanations are often dominated by the class labels; data points predicted as the same class would receive a similar set of explanations. In contrast, HD-Explain shows substantially higher coverage, providing a significant advantage for instance-level prediction explanation.

Regarding computation efficiency, while we have summarized the scalability limitation of the candidate methods in

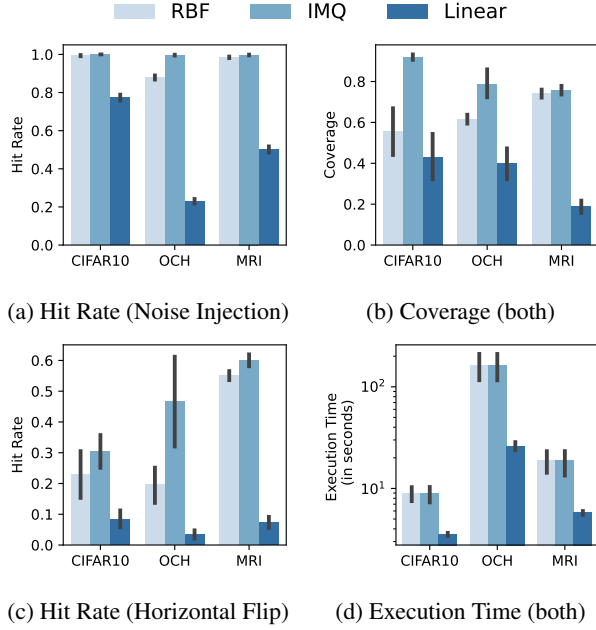


Figure 7: Quantitative explanation comparison among HD-Explainers with different kernel functions on all image classification datasets. Error bar shows 95% confidence interval.

Table 1, there was no computational efficiency evaluation conducted in previous works. To complement this lack, we recorded the wall clock execution time for previous quantitative experiments as shown in Figure 5(c). As expected, the Influence Function takes longer to return its explanation than other methods. HD-Explain and TracIn* are comparable. However, it is worth knowing that HD-Explain works on the whole model prediction, whereas TracIn* is configured only to compute the gradient of the predictive layer (due to the scalability issue of memory usage). Indeed, if we look at HD-Explain*, we note its computation time is much shorter than TracIn*. RPS shows a significant advantage in computation efficiency as it is 1) limited to the last layer of the neural network and 2) no auto-differentiation is needed for computing the training data influence.

We observe a similar trend in the other data augmentation scenario, Horizontal Flip, where computation time and coverage are roughly the same, as shown in Figure 6. However, we do notice that, as the outcome of image flipping, the raw feature (pixel) level similarity between \mathbf{x}_t and \mathbf{x}_i is destroyed. As an outcome, the HD-Explain that works on raw features suffers from performance deduction while other methods, including HD-Explain*, are less impacted. This observation suggests that choosing the layer of explanation might be considered in the practical usage of this approach.

4.3. Kernel Options

Our previous experiments used the Radial Basis Function (RBF) kernel by default. One may suggest another choice over kernels that better fit a particular application domain. In this experiment, we compare three well-known kernels on the three image classification datasets, including Linear, RBF, and Inverse Multi-Quadric (IMQ) kernels.

Figure 7 shows our experiment results under both data augmentation scenarios. We note that HD-Explain equipped with an IMQ kernel generally performs better than the RBF kernel regarding explanation quality (Hit Rate). The advantage is significant when the data augmentation scenario is Horizontal Flip (Figure 7 (c)), which appears more challenging than Noise Injection. In addition, the Coverage of explanation (Figure 7 (b)) aligns with the hit rate, where IMQ leads to a higher value. However, HD-Explain equipped with linear kernel runs much faster than the other options, as shown in Figure 7 (d), providing it with higher efficiency on large datasets. Indeed, if we cross-check the results with Figure 5, we note that even a Linear kernel is sufficient for HD-Explain to stand out from other baseline models considering its performance and efficiency. RBF and IMQ kernels often need similar computation time.

5. Conclusion

This paper presents HD-Explain, a Kernel Stein Discrepancy-driven neural classifier explanation method. The method is straightforward but powerful in terms of prediction explanation and data debugging tasks. The computation is efficient and can work with large machine learning models (e.g. ResNet) as a whole model explainer. Considering that many applications adopt pre-trained foundation models, we also introduced a variant of HD-Explain (HD-Explain*) that can work on the predictive layers such that the explanation would be limited to the model parts of interest. With empirical evidence demonstrated in this paper, we are confident that the method is practically effective for improving the transparency of Machine Learning predictive systems.

Impact Statements

This paper presents a prediction explanation method for neural network-based classifiers. While the ultimate goal of prediction explanation (and this work) is to improve the model transparency and trustworthiness, we note it could be misused to cause intentional prediction bias (e.g. removing high-influential training data points for specific purposes).

References

- Anik, A. I. and Bunt, A. Data-centric explanations: explaining training data of machine learning systems to promote transparency. In *Proceedings of the 2021 CHI Conference on Human Factors in Computing Systems*, pp. 1–13, 2021.
- Bae, J., Ng, N., Lo, A., Ghassemi, M., and Grosse, R. B. If influence functions are the answer, then what is the question? *Advances in Neural Information Processing Systems*, 35:17953–17967, 2022.
- Barp, A., Briol, F.-X., Duncan, A., Girolami, M., and Mackey, L. Minimum stein discrepancy estimators. *Advances in Neural Information Processing Systems*, 32, 2019.
- Barshan, E., Brunet, M.-E., and Dziugaite, G. K. Relatif: Identifying explanatory training samples via relative influence. In *International Conference on Artificial Intelligence and Statistics*, pp. 1899–1909. PMLR, 2020.
- Brophy, J., Hammoudeh, Z., and Lowd, D. Adapting and evaluating influence-estimation methods for gradient-boosted decision trees. *Journal of Machine Learning Research*, 24(154):1–48, 2023.
- Cai, C. J., Jongejan, J., and Holbrook, J. The effects of example-based explanations in a machine learning interface. In *Proceedings of the 24th international conference on intelligent user interfaces*, pp. 258–262, 2019.
- Chen, Y., Li, B., Yu, H., Wu, P., and Miao, C. Hydra: Hypergradient data relevance analysis for interpreting deep neural networks. In *Proceedings of the AAAI Conference on Artificial Intelligence*, volume 35, pp. 7081–7089, 2021.
- Chwialkowski, K., Strathmann, H., and Gretton, A. A kernel test of goodness of fit. In *International conference on machine learning*, pp. 2606–2615. PMLR, 2016.
- Frosst, N. and Hinton, G. Distilling a neural network into a soft decision tree. *arXiv preprint arXiv:1711.09784*, 2017.
- Gorham, J., Raj, A., and Mackey, L. Stochastic stein discrepancies. *Advances in Neural Information Processing Systems*, 33:17931–17942, 2020.
- Jacot, A., Gabriel, F., and Hongler, C. Neural tangent kernel: Convergence and generalization in neural networks. *Advances in neural information processing systems*, 31, 2018.
- Kattumannil, S. K. On stein’s identity and its applications. *Statistics & probability letters*, 79(12):1444–1449, 2009.
- Kim, B., Khanna, R., and Koyejo, O. O. Examples are not enough, learn to criticize! criticism for interpretability. *Advances in neural information processing systems*, 29, 2016.
- Koh, P. W. and Liang, P. Understanding black-box predictions via influence functions. In *International conference on machine learning*, pp. 1885–1894. PMLR, 2017.
- Korba, A., Aubin-Frankowski, P.-C., Majewski, S., and Ablin, P. Kernel stein discrepancy descent. In *International Conference on Machine Learning*, pp. 5719–5730. PMLR, 2021.
- Li, X.-H., Cao, C. C., Shi, Y., Bai, W., Gao, H., Qiu, L., Wang, C., Gao, Y., Zhang, S., Xue, X., et al. A survey of data-driven and knowledge-aware explainable ai. *IEEE Transactions on Knowledge and Data Engineering*, 34(1):29–49, 2020.
- Lim, B. Y., Yang, Q., Abdul, A. M., and Wang, D. Why these explanations? selecting intelligibility types for explanation goals. In *IUI Workshops*, 2019.
- Liu, Q. and Wang, D. Stein variational gradient descent: A general purpose bayesian inference algorithm. *Advances in neural information processing systems*, 29, 2016.
- Liu, Q., Lee, J., and Jordan, M. A kernelized stein discrepancy for goodness-of-fit tests. In *International conference on machine learning*, pp. 276–284. PMLR, 2016.
- Nam, C. S., Jung, J.-Y., and Lee, S. *Human-Centered Artificial Intelligence: Research and Applications*. Academic Press, 2022.
- Park, S. M., Georgiev, K., Ilyas, A., Leclerc, G., and Madry, A. Trak: Attributing model behavior at scale. In *International Conference on Machine Learning (ICML)*, 2023.
- Peterson, L. E. K-nearest neighbor. *Scholarpedia*, 4(2): 1883, 2009.
- Pruthi, G., Liu, F., Kale, S., and Sundararajan, M. Estimating training data influence by tracing gradient descent. *Advances in Neural Information Processing Systems*, 33: 19920–19930, 2020.
- Schioppa, A., Zablotskaia, P., Vilar, D., and Sokolov, A. Scaling up influence functions. In *Proceedings of the AAAI Conference on Artificial Intelligence*, volume 36, pp. 8179–8186, 2022.
- Sui, Y., Wu, G., and Sanner, S. Representer point selection via local jacobian expansion for post-hoc classifier explanation of deep neural networks and ensemble models. *Advances in neural information processing systems*, 34: 23347–23358, 2021.

- Tsai, C.-P., Yeh, C.-K., and Ravikumar, P. Sample based explanations via generalized representers. *Advances in Neural Information Processing Systems.*, 36, 2023.
- Yang, J., Liu, Q., Rao, V., and Neville, J. Goodness-of-fit testing for discrete distributions via stein discrepancy. In *International Conference on Machine Learning*, pp. 5561–5570. PMLR, 2018.
- Yeh, C.-K., Kim, J., Yen, I. E.-H., and Ravikumar, P. K. Representer point selection for explaining deep neural networks. *Advances in neural information processing systems*, 31, 2018.
- Zhou, J., Gandomi, A. H., Chen, F., and Holzinger, A. Evaluating the quality of machine learning explanations: A survey on methods and metrics. *Electronics*, 10(5):593, 2021.

A. Problem Definition Recap

We consider the task of explaining the prediction of a differentiable classifier $f : \mathbb{R}^d \rightarrow \mathbb{R}^l$, given inputs test sample $\mathbf{x}_t \in \mathbb{R}^d$, where d denotes the input dimension and l denotes the number of classes. Specifically, we are interested in explaining a prediction of a model $f(\cdot)$ by returning a subset of its training samples $D = \{(\mathbf{x}_i, y_i)\}_{i=1}^n$ that has strong predictive support to the prediction of test point \mathbf{x}_t . While not explicitly stated in the main paper, we treat example-based prediction explanation as a function $\psi(f, D, \mathbf{x}_t) : \mathcal{F} \times \mathcal{D} \times \mathbb{R}^d \rightarrow \{\mathbb{R}^d, \mathbb{R}^l\}^k$ such that it takes a trained model f , a training dataset D , and an arbitrary test point \mathbf{x}_t as inputs and output top- k training samples as explanations.

B. Additional Derivation of Kernelized Stein Discrepancy

While Stein's Identity has been well described in many previous works (Liu et al., 2016; Liu & Wang, 2016; Chwialkowski et al., 2016), we briefly recap some key derivations in this paper to seek for self-contained.

As mentioned in the main paper, Stein's Identity states that, if a smooth distribution $p(x)$ and a function $\phi(x)$ satisfy $\lim_{\|x\| \rightarrow \infty} p(x)\phi(x) = 0$, we have

$$\mathbb{E}_{x \sim p}[\phi(x)\nabla_x \log p(x) + \nabla_x \phi(x)] = \mathbb{E}_{x \sim p}[\mathcal{A}_p \phi(x)] = 0, \quad \forall f.$$

Intuitively, by using integration by part rules, we can reveal the original assumption from the derived expression such that

$$\int_x \phi(x)\nabla_x \log p(x) + \nabla_x \phi(x)dx = p(x)\phi(x) \Big|_{-\infty}^{+\infty}$$

Stein Discrepancy measures the difference between two distributions q and p by replacing the expectation of distribution p term in Stein's Identity expression with distribution q , which reveals the difference between two distributions by projecting their score functions (gradients) with the function $\phi(x)$

$$\max_{\phi \in \mathcal{F}} \mathbb{E}_{x \sim q}[\mathcal{A}_p \phi(x)] = \max_{\phi \in \mathcal{F}} \mathbb{E}_{x \sim q}[\mathcal{A}_p \phi(x)] - \underbrace{\mathbb{E}_{x \sim q}[\mathcal{A}_q \phi(x)]}_{=0} = \max_{\phi \in \mathcal{F}} \mathbb{E}_{x \sim q} \left[\underbrace{\phi(x)}_{\text{projection coefficients}} \underbrace{(\nabla_x \log p(x) - \nabla_x \log q(x))}_{\text{score function difference}} \right]$$

Clearly, the choice of projection coefficients (function $\phi(x)$) term is critical to measure the distribution difference.

Kernelized Stein Discrepancy (KSD) addresses the task of searching function ϕ by treating the above challenge as an optimization task where it decomposes the target function ϕ with linear decomposition such that

$$\max_{\phi \in \mathcal{F}} \mathbb{E}_{x \sim q}[\mathcal{A}_p \phi(x)] = \max_{\phi \in \mathcal{F}} \mathbb{E}_{x \sim q}[\mathcal{A}_p \sum_i w_i \phi_i(x)] = \max_{\phi \in \mathcal{F}} \sum_i w_i \mathbb{E}_{x \sim q}[\mathcal{A}_p \phi_i(x)],$$

with linear property of Stein operator \mathcal{A}_p . The linear decomposition path is the way to reduce the optimization task into looking for a finite number of the base functions $\phi_i \in \mathcal{F}$ whose coefficient norm is constraint to 1 ($\|\mathbf{w}\|_{\mathcal{H}} \leq 1$). KSD takes \mathcal{F} to be the unit ball of a reproducing kernel Hilbert space (RKHS) and leverages its reproducing property such that $\phi(x) = \langle \phi(\cdot), k(x, \cdot) \rangle$, which in turn transforms the maximization objective of the Stein Discrepancy into

$$\max_{\phi} \langle \phi(\cdot), \mathbb{E}_{x \sim q}[\mathcal{A}_p k(\cdot, x)] \rangle_{\mathcal{H}}, \quad \text{s.t. } \|\phi\|_{\mathcal{H}} \leq 1.$$

The optimal ϕ is therefore a normalized version of $\mathbb{E}_{x \sim q}[\mathcal{A}_p k(\cdot, x)]$. Hence, KSD is defined as the optimal between the distribution p and q with the optimal solution of ϕ

$$\mathbb{S}(q, p) = \mathbb{E}_{x, x' \sim q}[\kappa_p(x, x')], \quad \text{where} \quad \kappa_p(x, x') = \mathcal{A}_p^x \mathcal{A}_p^{x'} k(x, x').$$

C. Discussion: Intuition on why HD-Explain works

In HD-Explain, the key metric on measuring the predictive supports of a test point \mathbf{x}_t given a training data $(\mathbf{x}_i, \mathbf{y}_i)$ is the KSD defined kernel $\kappa_{\theta}([\mathbf{x}_t || \hat{\mathbf{y}}_t], [\mathbf{x}_i || \mathbf{y}_i])$, where $\hat{\mathbf{y}}_t$ denotes the predicted class label by model f_{θ} in one-hot encoding. By definition, the kernel $\kappa_{\theta}((\mathbf{x}_a, y_a), (\mathbf{x}_b, y_b)) = k_{\theta}(a, b)$ between two data points can be decomposed into four terms

$$\underbrace{\text{trace}(\nabla_a \nabla_b k(a, b))}_{\textcircled{1}} + \underbrace{k(a, b) \nabla_a \log P_{\theta}(a)^{\top} \nabla_b \log P_{\theta}(b)}_{\textcircled{2}} + \underbrace{\nabla_a k(a, b)^{\top} \nabla_b \log P_{\theta}(b)}_{\textcircled{3}} + \underbrace{\nabla_b k(a, b)^{\top} \nabla_a \log P_{\theta}(a)}_{\textcircled{4}}.$$

We examine the effect of each term as follows:

- ①: We note that the first term is often a similarity bias of raw data points given a specified kernel function. In particular, for the RBF kernel $k(a, b) = \exp(-\gamma||a - b||^2)$, the first term is simply $\sum_i^{d+l} 2\gamma k(a, b)$, where $d + l$ refers to the sum of input and output (in one-hot) dimensions of a data point. Intuitively, the term shows how similar the two data points are given the RBF kernel. For linear kernel $k(a, b) = a^\top b$, on another hand, the first term is simply $d + l$ as a constant bias term, which does not deliver any similarity information between the two data points.
- ②: The second term reflects the similarity between two data points in the context of the trained model. In particular, considering the sub-term $\nabla_a \log P_\theta(a)^\top \nabla_b \log P_\theta(b)$, based on our derivation in Equation 2 (in the main paper), we note it is equivalent to

$$[\nabla_{\mathbf{x}_a} \log f_\theta(\mathbf{x}_a)_{y_a} || f_\theta(\mathbf{x}_a)]^\top [\nabla_{\mathbf{x}_b} \log f_\theta(\mathbf{x}_b)_{y_b} || f_\theta(\mathbf{x}_b)] = \underbrace{\nabla_{\mathbf{x}_a} \log f_\theta(\mathbf{x}_a)_{y_a}^\top \nabla_{\mathbf{x}_b} \log f_\theta(\mathbf{x}_b)_{y_b}}_{\text{similarity of scores (input gradients)}} + \underbrace{f_\theta(\mathbf{x}_a)^\top f_\theta(\mathbf{x}_b)}_{\text{similarity of predictions}},$$

where both terms could be viewed as similarity between data points in the context of trained model.

- ③-④: Both of the last two terms examine the alignment between the score of one data point and the kernel derivative of another data point. We conjecture that this alignment reflects how a test prediction would change if there is a training data point present closer to it than before.

D. Dataset Details

Table 2: Summary of datasets used in the paper.

Dataset	Application	Type	# Size	# Feature Dimension	# Number of Classes	Duplicated Samples	Public Dataset
Two Moons	Synthetic	2D Numeric	500	2	2	No	Shared with code
Rectangulars	Synthetic	2D Numeric	500	2	3	No	Shared with code
CIFAR-10	Classification Benchmark	Image	60,000	$32 \times 32 \times 3$	10	No	Yes
Overian Cancer	Histopathology (Private)	Image	20,000	$128 \times 128 \times 3$	5	Yes	No
Brain Tumor	MRI Benchmark	Image	7,023	$128 \times 128 \times 3$	4	Yes	Yes

In this paper, we conducted our experiments on five datasets – two synthetic and three benchmark image classification datasets. As the work concerns the trustworthiness of the machine learning model in high-stakes applications, we also introduced medical diagnosis datasets to provide more insight into the potential benefit the proposed work introduced. To train the target machine learning models, we conducted data augmentations to increase the number of training data samples, including random cropping, rotation, shifting, horizontal flipping, and noise injection. Table 2 summarizes more details about the datasets.

E. Data Debugging

Before describing the data debugging setting of this paper, we want to recap that the data debugging functionality is a side effect/benefit of HD-Explain, which is not our main proposal. Indeed, using the prediction explanation method as a data debugging tool is still under investigation since it might be over-claimed due to the over-regularized setting in previous works (e.g. Binary classification tasks). While we relaxed some settings, we don’t claim it practical for real-world applications.

The data debugging task in this paper is a data sample retrieval task where we retrieve samples that intentionally flipped their classification labels. Higher Precision and Recall of the retrieval reflects higher performance of data debugging.

For the HD-Explain (and its variant HD-Explain*), the retrivial order is determined by the values of the diagonals of the KSD-defined kernel matrix, $\kappa_\theta(a, a)$ for all $a \in D$. This setting is very similar to how the Influence function does the data debugging with the self-influence of a data sample. Indeed, $\kappa_\theta(a, a)$ could be treated as a self-influence that does not rely on model parameters.

Now, we describe our data debugging experiments to highlight the self-explanatory ability of candidate methods on the training data. In particular, we generalized previous research’s binary classification-based data debugging experiment into a multi-classification scenario, where we randomly flip labels of 100 training data points at each run. We adopt standard information retrieval metrics, Precision and Recall, that measure how likely the candidate methods can retrieve the mislabeled training data points. Figure 8 shows our experimental results. While HD-Explain on the entire model has

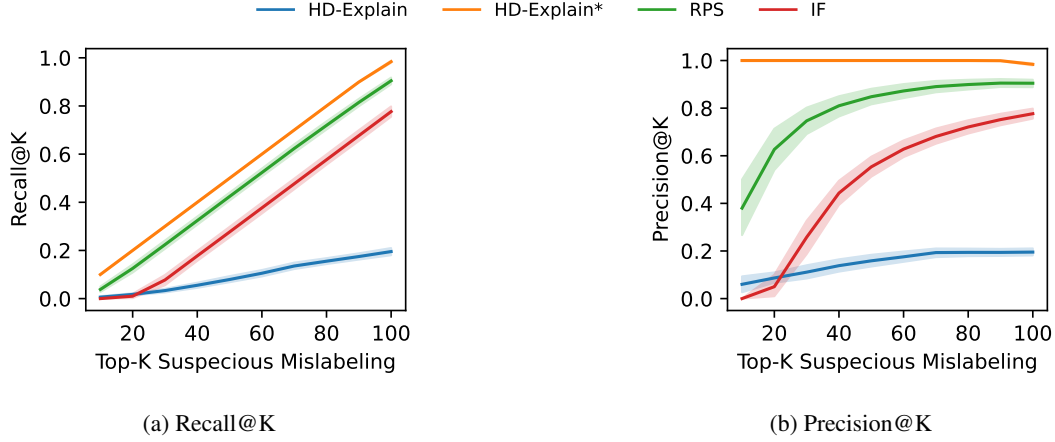


Figure 8: Data debugging comparison among candidate methods on CIFAR-10 dataset. Results collected from 30 independent runs. Error bar shows 95% confidence interval.

little data debugging ability, its variant on the last layer offers outstanding performance compared to the other last-layer explanation methods. Note, the data debugging functionality is a side effect/benefit of HD-Explain, which is not our main proposal

F. HD-Explain*

In the main paper, we briefly mentioned HD-Explain* as an HD-Explain variant to match the last layer setting of other baseline models (e.g. RPS). The HD-Explain* is a simple change of HD-Explain in terms of using data representations (the output of the last non-predictive layer of the neural classifier) rather than the raw features. Specifically, we assume a neural network model f_θ could be decomposed into two components $f_{\theta_2} \cdot f_{\theta_1}$, where f_{θ_1} is a representation encoder and f_{θ_2} is a linear model for prediction. With this decomposition, we define the KSD kernel function for HD-Explain* as

$$\begin{aligned} \kappa_\theta((f_{\theta_1}(\mathbf{x}_a), y_a), (f_{\theta_1}(\mathbf{x}_b), y_b)) &= \mathcal{A}_{\theta_2}^a \mathcal{A}_{\theta_2}^b k(a, b) \\ &= \nabla_a \nabla_b k(a, b) + k(a, b) \nabla_a \log P_{\theta_2}(a) \nabla_b \log P_{\theta_2}(b) + \nabla_a k(a, b) \nabla_b \log P_{\theta_2}(b) + \nabla_b k(a, b) \nabla_a \log P_{\theta_2}(a), \end{aligned}$$

where we define $a = (f_{\theta_1}(\mathbf{x}_a), y_a)$ and $b = (f_{\theta_1}(\mathbf{x}_b), y_b)$ for short. This setting reduces the prediction explanation to the last layer of the neural network in a similar fashion to RPS.